Advanced Lab Course: Particle Physics

Sillicon Strip Detector

Leander Flottau
leander.flottau@tu-dortmund.de

Ajeesh Garg
smajgarg@tu-dortmund.de

20. July 2024

TU Dortmund University – Department of Physics

Contents

1 Introduction

The CERN nuclear research center in Geneva has a circumference of around 27 kilometers and is home to four large experiments, namely ALICE, LHCb, CMS, and ATLAS, where protons are made to collide. This report revolves around the ATLAS detector where particles collide in a cylindrical beam tube. The ATLAS detector is built in several layers with the inner detector (ID) being the innermost part where the particles collide. The inner detector consists of a pixel detector and a Silicon Strip Detector (SCT). The aim of this experiment is to study the functioning of a silicon semiconductor detector of ATLAS using the Educational Alibava System (EASy) produced by Alibava Systems. In this task, a radioactive source emitting beta radiation is kept in a sufficiently shielded environment.

2 ATLAS Detector

The ATLAS detector is one of the four experiments at CERN. It consists of a cylindrical tube where protons collide. The detector is built in several layers with the innermost layer consisting of a pixel detector and silicon strip detectors.

2.1 Pixel Detector and Silicon Strip Detectors

The pixel detector has a higher spatial resolution due to its highly segmented nature but is more expensive to produce compared to the silicon strip detector. Despite their higher cost, pixel detectors are used in the innermost layer of the ATLAS detector. The second innermost layer consists of four double-layer silicon strip detectors twisted at an angle of 40 mrad. These silicon strip detectors directly connected to the pixel detector improve the overall spatial resolution by their combination with the pixel detectors. The original semiconductor strip consists of 4088 individual modules each containing 768 strips. For our analysis, the apparatus we are using consists of 128 individual strips.

2.2 Determination of Energy of Particles

The innermost detector is surrounded by a magnetic coil and this perpendicular magnetic field causes charged particles to deflect in curved paths. This bending of particles under the influence of a magnetic field helps determine the momentum and charge of the charged particles. Behind the magnet, we have the calorimeter which determines the energy of the particles.

$$E^2 = p^2 + m^2 \tag{1}$$

By using Einstein's energy equation, we can determine the mass of the particles. The mass being a unique characteristic of the particle can be used to identify the type of particle.

3 Semiconductor Detectors

Silicon chip detectors are made out of semiconductors. Semiconductors are materials which have electrical properties between those of conductors and insulators. The key characteristic that defines a semiconductor is its band gap which is the energy difference between the valence band (the highest energy band that is fully occupied by electrons) and the conduction band (the lowest energy band that is empty). For semiconductors, this gap is of the order of electron volts (eV).

The most commonly used semiconductor material is silicon which has a band gap of about 1.12 eV at room temperature. This band gap is small enough to allow electrons to jump from the valence band to the conduction band under certain conditions, e.g., by increasing temperature or by adding certain impurities.

3.1 Doping

This process of changing electrical properties of semiconductors by adding impurities is called doping. Doping involves adding a small amount of impurity atoms to the semiconductor crystal. Depending on the type of impurity added, the semiconductor becomes either n-type or p-type.

3.1.1 N-type Semiconductors

When atoms with five valence electrons such as Arsenic or phosphorus are added to silicon, they introduce extra electrons into the conduction band. These extra electrons increase the material's conductivity. Since these electrons are negative charge carriers, the semiconductor is termed n-type. Since this electron could move freely in the lattice if it were not bound to the Coulomb interactions of the atomic body. Arsenic that is doped in silicon is therefore referred to as a donator.

3.1.2 P-type Semiconductors

On the other hand, when the crystal is doped with an element of three electrons, it leads to the generation of vacant spaces in the crystal. These holes can move through the lattice and act as positive charge carriers and the semiconductor is termed p-type.

3.2 Temperature Dependence

As the temperature increases, some electrons gain enough thermal energy to jump from the valence band to the conduction band leaving behind holes in the valence band. These holes act as positive charge carriers. The presence of these free electrons and holes enables intrinsic conduction. However, the intrinsic conductivity of silicon is relatively quite lower than conductors.

3.3 The p-n Junction

When a p-type semiconductor and an n-type semiconductor are joined together, a p-n junction is formed. At the junction, electrons from the n-type material diffuse into the p-type material and recombine with holes. This diffusion process leaves behind positively charged donor atoms in the n-type region and negatively charged acceptor atoms in the p-type region. A dynamic equilibrium between diffusion and opposite electrical drift is established. Further creating a region devoid of free charge carriers known as the depletion region. The silicon strip detectors used in the ATLAS experiment also work on the principle of PN junction diode.

4 The Experimental Setup

The experimental setup consists of three main parts which are control unit, the detector unit, and the computer. As the name suggests, the control unit controls the detector by controlling the supply of voltage and current to the detector system, and the detector system detects the signal and supplies it to the computer unit.

4.1 Detector Unit

The detector unit contains the silicon strip sensor and its associated readout electronics. The silicon sensor operates on the principle of a p-in-n sensor where the base is an n-doped silicon layer with 128 p-doped strips embedded on the top. These strips are covered with a silicon oxide layer to prevent leakage current. The sensor's configuration allows for the precise localization of deposited charge by insulating the strips from one another. The BEETLE chip used in the LHCb experiment is employed here to amplify incoming charge signals, convert them into digital signals, and then convert them into ADC counts.

The sensor must be fully depleted for efficient measurement with the depletion voltage (U_{dep}) which was measured to be 130 V. In the figure, we can see the current almost saturates after the depletion voltage. After the determination of the depletion voltage, the better here for the pearls for all that 128 trips by taking an average over 1000 even was calculated.

The sensor is mounted on a sliding platform with two positions: (L) for laser measurements and (Q) for source measurements.

4.2 Control Unit

The control unit connected to the detector unit via a ribbon cable supplies the necessary voltage and transmits data. It is also connected to a computer via a USB cable for data acquisition and control through the Alibava-gui software. The control unit allows for the adjustment of bias voltage using a rotary knob labeled "Diode Bias" with the current leakage monitored via an ammeter.

5 Analysis

First the noise of the detector as is examined. Afterwards there are several calibration measurements made. Then the detector response is examined using a laser and a radioactive source.

5.1 Current-voltage characteristic

As a first step the depletion voltage is to be determined using the current-voltage characteristic, which is generated by measuring the leakage current while slowly increasing the external voltage from 0 V to 200 V in 10 V steps. The resulting curve is displayed in 1.

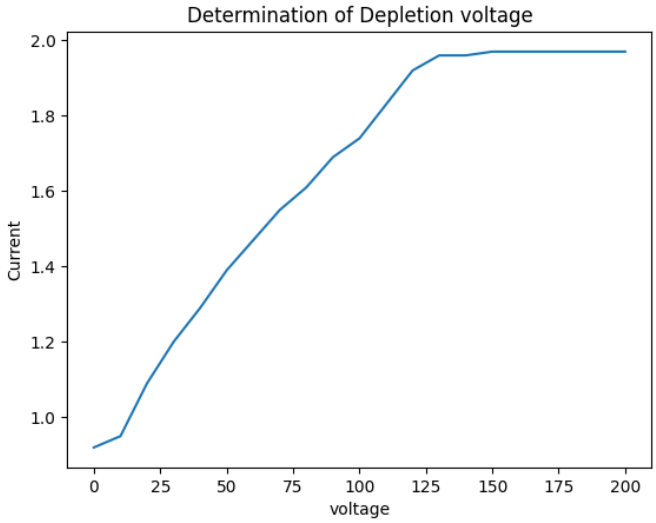

Figure 1: Current-voltage characteristic of the sillicon strip sensor

The plateu is reached at roughly 125 V which is relatively high compared to the depletion voltage of 80 V. This discrepancy is most likely caused by the low time intervalls between the individual measuring points.

5.2 Pedestal and noise

Aside from the signal the counts measured by the detector are effected by two different types of background, both of which can be determined by a distinct measurement.

$$ADC(i,k) = P(i) + D(k) + signal(i,k) \tag{2}$$

The pedestal $P(i)$ is a type of background that is specific to each strip i. It can be determined for every strip from a background measurement without signal as:

$$P(i) = \frac{1}{N}\sum_{k}^{N}(ADC(i,k)) \tag{3}$$

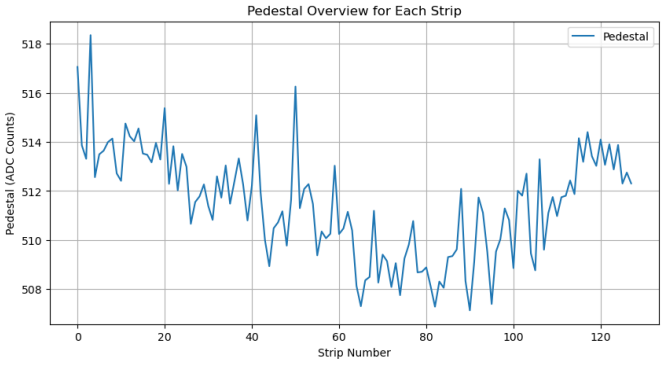

Figure 2: Pedestal depending on the channel

with the number of events N. The Pedestal in depending on the channel can be viewed in Figure 2

Unlike the Pedestal the common shift $D(k)$ is an event specific background that effects every strip equally. It can also be determined from the background measurement

$$D(k) = \frac{1}{128} \sum_{i}^{128} (ADC(i,k) - P(i)) \tag{4}$$

The common shift for every event as well as the distribution of the common shift is

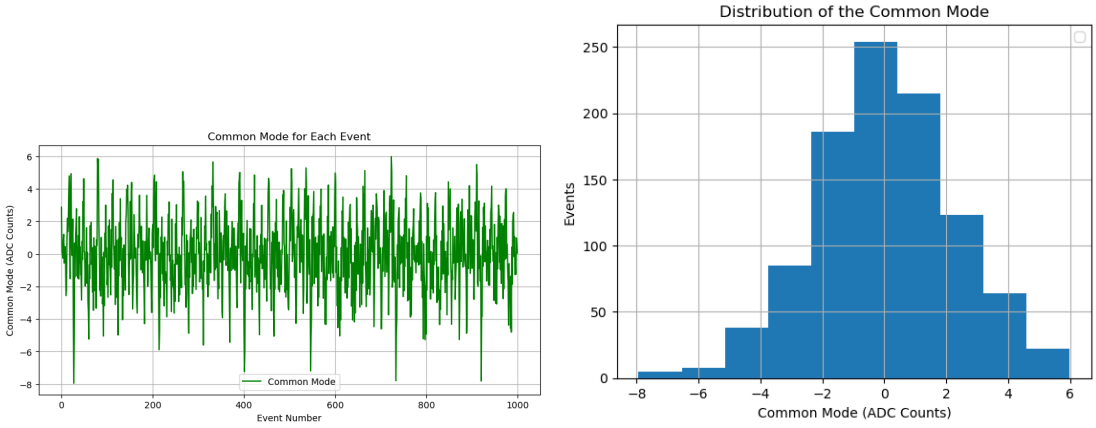

Figure 3: Common shift depending on the event (left), and common mode distribution (right)

displayed in 3.

Combining the information from the pedestal and the noise allows for the calculation of the common noise

$$Noise(i) = \sqrt{\frac{1}{N-1} \sum_{k}^{N} (ADC(i,k) - P(i) - D(k))^2} \tag{5}$$

The resulting noise for every strip is displayed in 4.

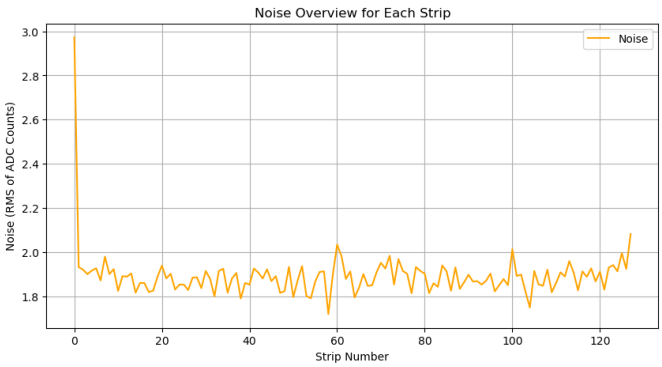

Figure 4: Common noise depending on the channel

5.3 Calibration

Before the actual measurements take place the detector is calibrated. An essential part of this is determining the optimal delay between signal and readout. From the resulting

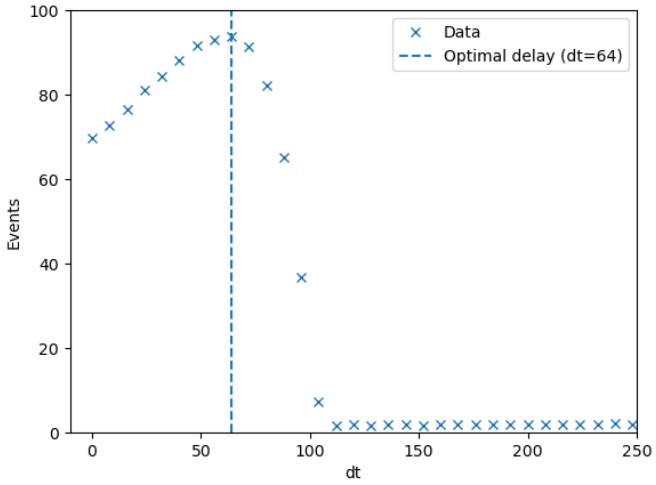

Figure 5: Signal depending on the delay

calibration curve in Figure 5 the optimal delay time can be determined to be 64 ns.

Additionally a different calibration measurement can be used to examine how the measured counts depend on the charge flow through the detector. This is done by determing the number of pulses associated with the output signal for five different readout channels. The resulting calibration curves of five different strips are depicted in Figure 6. All five strips show almost identical results. The mean value of the curves can also be fitted using 4th-degree polynomial, which can also be seen in 6. To get a good

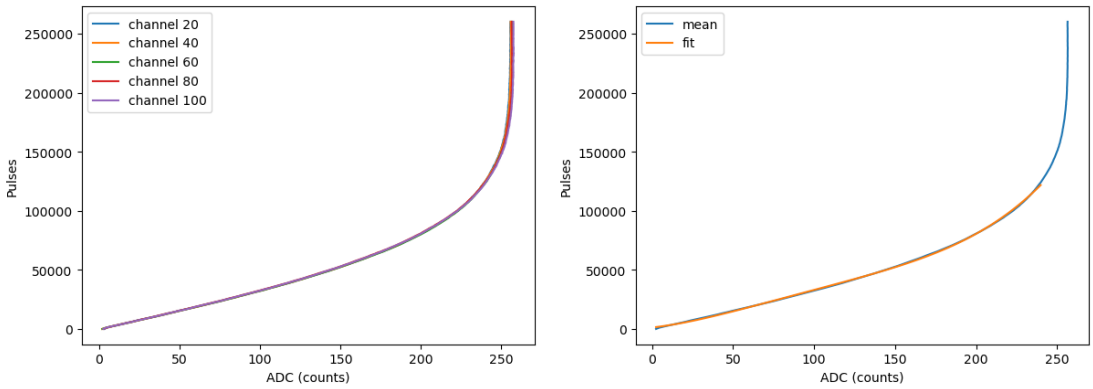

Figure 6: Calibration curve of the five selected strips (left) and curve of the mean value with the corresponding 4th-degree polynomial fit

result with the chosen function the range has to be restricted to ADC-counts smaller than $ADC = 240$.

In addition to the calibration curves presented so far a measurement was made for an external voltage of $U = 0\,\mathrm{V}$ for one of the selected strips. The resulting curves are

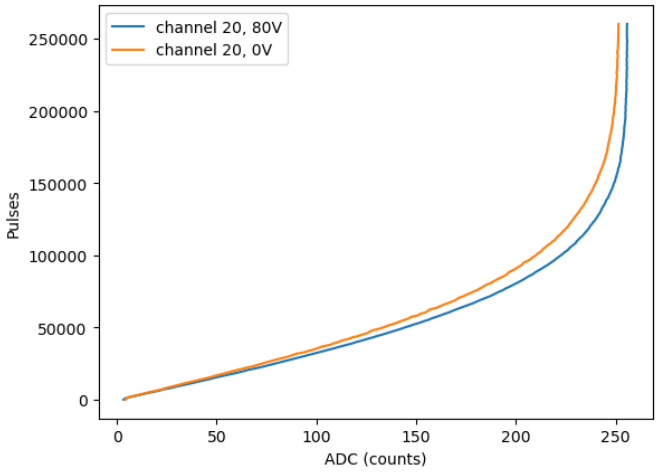

Figure 7: Calibration curves for channe 20 with 80 V and 0 V external potential

compared in Figure 7. Without an external voltage a higher number of pulses is required to achieve the same output signal because the effective region, in which the detector can track events, is smaller.

5.4 Properties of the detector

Using a laser the properties of the detector and its spacial strucutre can be examined. This is achieved by performing 35 measurements for different horizontal positions of the laser. Before performing this measurement the optimal delay time of the laser has to

be determined similarly to the previous section. The resulting calibration curve can be

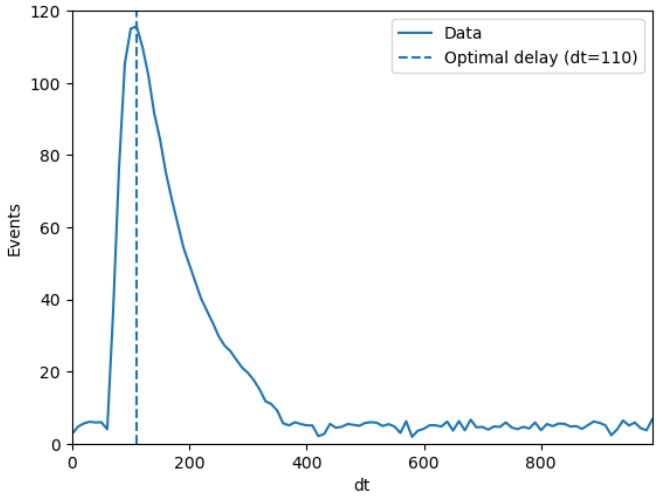

Figure 8: Optimal delay curve for the laser

examined in Figure 8. The determined optimal delay is 110 ns.

The most relevant channels for the measurement can be determined by plotting the first three of the 35 measurements depending on the channel. Based on the result displayed

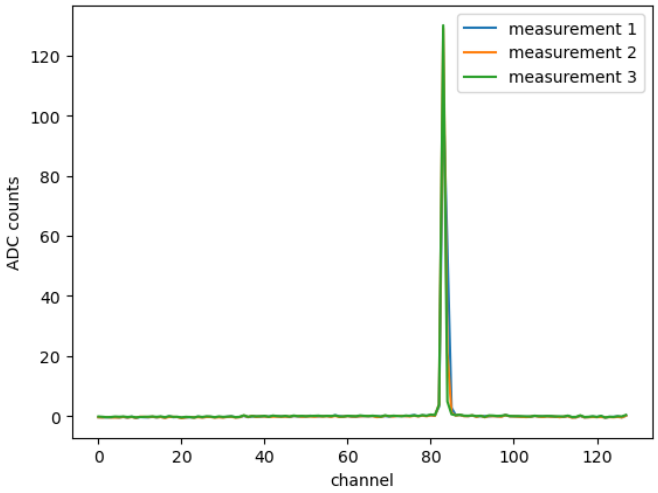

Figure 9: Signal depending on the channel for the first three measurement

in 9 it can be concluded that the channels 80-85 are likely the relevant ones to the measurement.

The metallisation in the middle of the individual strips reflects the laser and makes a signal measurement impossible. This property can be used to inestigate the structure of the strips. To do this the position dependend signal of the most relevant strips is depicted

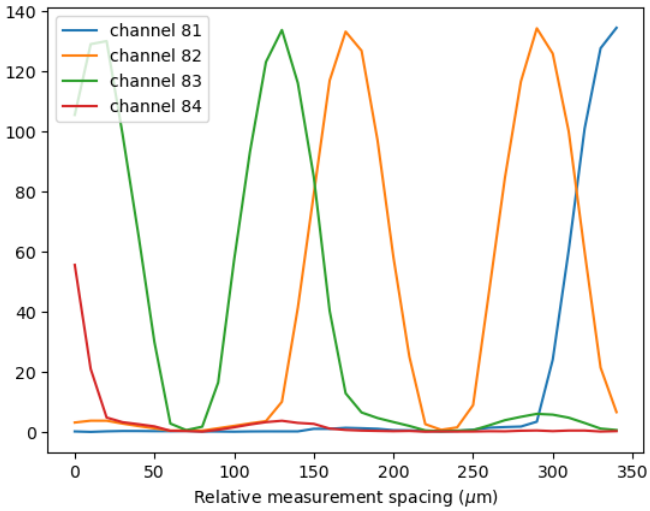

Figure 10: ADC counts depending on the horizontal position of the laser for the four most relevant channels

in Figure 10. The local minima in the individual measurements signal the laser hitting the center of the strip. Using this the distance of the minima of the channels 82 and 83 can be used to determine the spacing of the strips to be $d_{strips} = 160\,\mu\text{m}$. Additionally the extension of the laser on the strips can be determined from the distance between the minimum and the maximum to be $D_{laser} = 50\,\mu\text{m}$.

5.5 Charge Collection Efficiency

The charge collection efficiency of the detector is defined as the fraction of produced electron positron pairs that are detected and depends on the applied external voltage.

5.5.1 Laser

For the laser the charge collection efficiency can be calculated via the formula:

$$CCE(U) = \frac{1 - e^{\frac{d(U)}{a}}}{1 - e^{\frac{D}{U}}} \tag{6}$$

with the thickness of the detector $D = 300\,\mu\text{m}$, the penetration depth of the laser a and the thickness of the depletion zone $d(U)$ defined as:

$$d(U) = D\sqrt{\frac{U}{U_{dep}}} (if U < U_{dep}) \tag{7}$$

$$d(U) = D (if U \geq U_{dep}) \tag{8}$$

The charge collection efficiency is measured depending on the external voltage. The

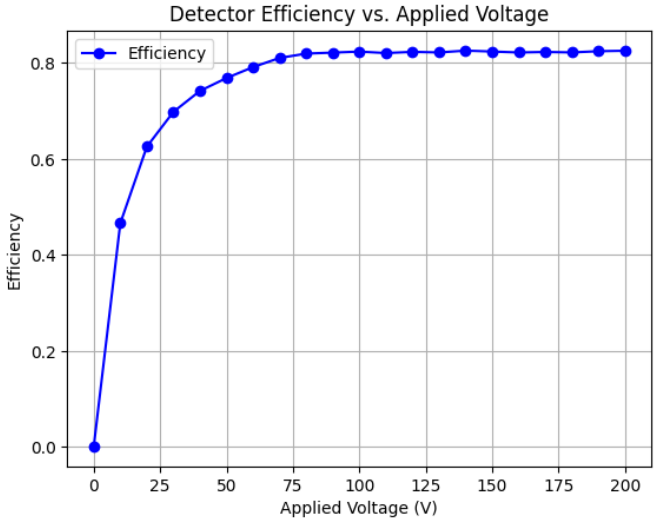

Figure 11: Charge collection efficiency of the detector using the laser

result is depicted in 11. Unlike the current voltage characteristic the plateu in this measurement is consistent with the depletion voltage given by the manufacturer. In the

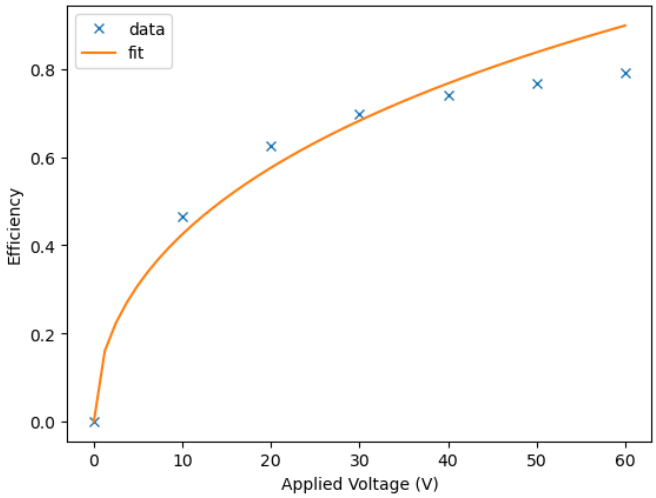

Figure 12: Charge collection efficiency and corresponding fit for low voltages

low voltage area the data can be fitted using the given formula for the CCE to determine the penetration depth of the laser as shown in Figure 12. The fit results in a value of $a = (489.00 \pm 0.04)\,\mu\text{m}$ for the penetration depth.

5.5.2 Radioactive source

In addition to the laser the charge collection efficiency is also examined using Sr^{90} as a radioactive β^- source. The mean cluster energy depending on the applied external

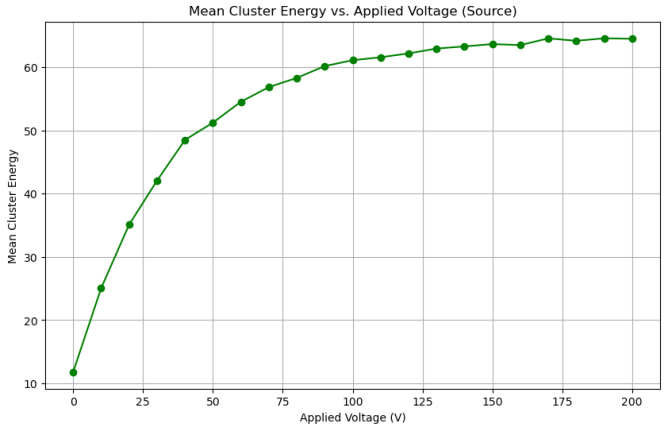

Figure 13: Mean cluster energy depending on the applied external voltage

voltage is displayed in Figure 13. Compared to the laser measurement the cluster energy increases more slowly and does not reach a platteau at the depletion voltage. The cause for this is that the emmission of a radioactive source is stochastic in nature and therefore much less precise than the laser.

5.6 Big source measurement

In the last measurement the emmission of the radioactive β^- source is more closely examined during a longer measurement containing a total of 1000000 events. From the

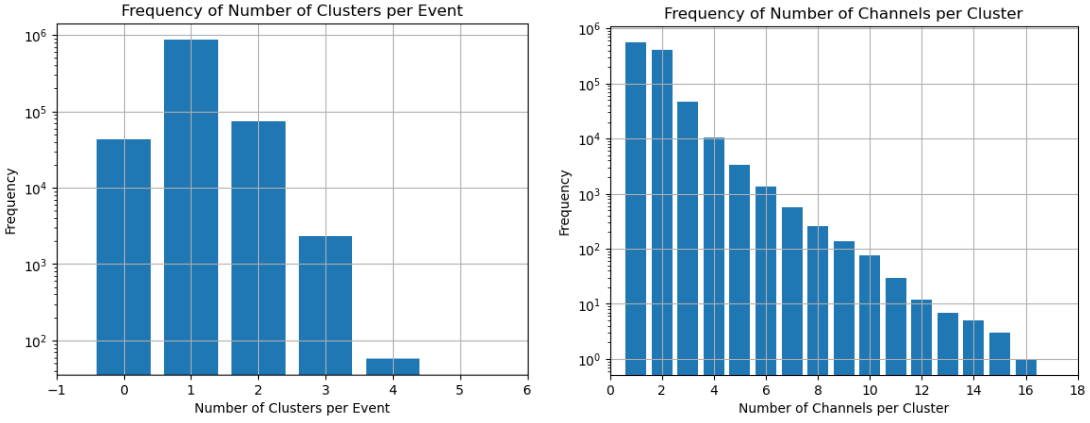

Figure 14: Number of clusters per event (left) and number of channels per cluster (right)

measurement first the number of channels per cluster and the number of clusters per event are determined as shown in Figure 14.

In the next step the number of hits for each channel can be examined. The result

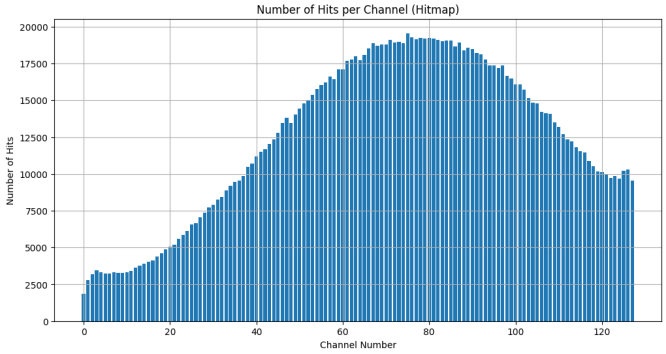

Figure 15: Number of events for every channel

is depicted in figure 15. The maximum is around channel 80 where there is the best alignment with the source.

At last the energy spectrum of the measurement can be determined. To convert the

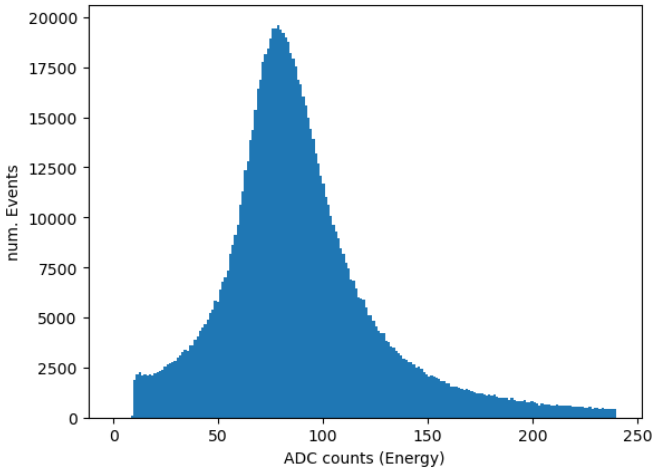

Figure 16: ADC spectrum of the big source measurement

spectrum of the *ADC* counts depicted in 16 the polynomial fit from the calibration measurement can be used to convert the *ADC* counts to the corresponding number of pulses. Together with the energy required to generate an electron-hole pair in sillicon 3.6 eV an actual energy spectrum can be generated. The result is displayed in 17. Using this data the mean value $\mu = (108.23 \pm 0.06)\,\mathrm{keV}$ and the most probable value $MPV = 88.3\,\mathrm{keV}$ (after rounding to the first decimal) can be determined. As to be expected the distribution approximately follows a Landau-distribution where the most probable value is smaller than the mean.

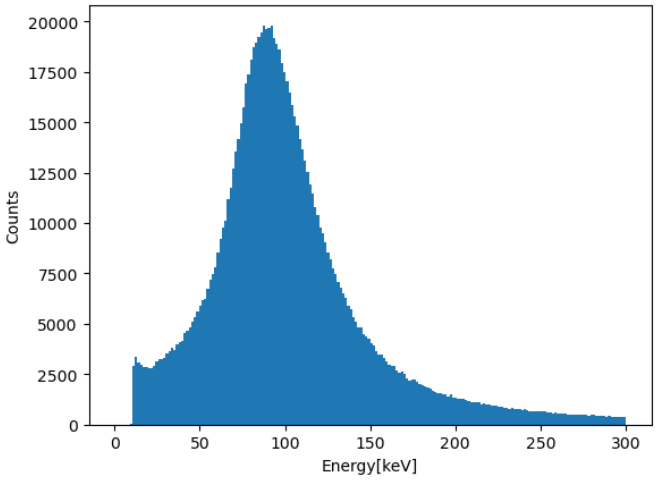

Figure 17: ADC spectrum of the big source measurement

6 Conclusion

With the intention of accurately characterising the sillicon strip detector first several calibration measurements were done, to accurately describe the background and examine the connection between *ADC*-counts and deposited energy. A current-voltage characteristic was measured showing a significantly higher depletion voltage than expected for this detector, which can most likely be explained by the measuring periods beeing too short

Afterwards the structure of the detector was examined using a 980 nm laser. While the resulting apcing of the strips of $d_{strips} = 160\,\mu\text{m}$ aligns well with the value given by the manufacturer, the measured diameter of the laser $D_{laser} = 50\,\mu\text{m}$ is much higher than the manufacturer value of 20 µm. This could be explained by the laser beeing defocused during the calibration to get a better signal.

The values for the charge collection efficiency also align well with the theoretical expectation. The penetration depth of the laser $a = (489.00 \pm 0.04)\,\mu\text{m}$ can be determined with a very low uncertainty, but is again significantly higher than to be expected of a laser with this wavelength. This might be caused by too many points beeing considered for the fit.

The measurement of the energy spectrum of the radioactive source shows the expected approximate Landau distribution in good agreement with the theory.

References

[1] *V15: Characterization of silicon strip sensors*. Fakultät Physik, TU Dortmund.